J. Fluid Mech. (2013), *vol.* 736, *pp.* 351–365.
doi:10.1017/jfm.2013.496

Threshold shear stress for the transition between tumbling and tank-treading of red blood cells in shear flow: dependence on the viscosity of the suspending medium

Thomas M. Fischer† and Rafal Korzeniewski

Department of Physiology, RWTH Aachen University, Pauwelsstr. 30, 52074 Aachen, Germany

(Received 18 January 2013; revised 4 July 2013; accepted 15 September 2013;
first published online 6 November 2013)

Red blood cells are the subject of diverse studies. One branch is the observation and theoretical modelling of their behaviour in a shear flow. This work deals with the flow of single red cells suspended in solutions much more viscous than blood plasma. Below a critical shear rate ($\dot{\gamma}_t$) the red cells rotate with little change of their resting shape. Above that value they become elongated and aligned in the shear field. We measured $\dot{\gamma}_t$ at viscosities (η_0) ranging from 10.7 to 104 mPa s via observation along the vorticity of a Poiseuille flow in a glass capillary; $\eta_0\dot{\gamma}_t$ decreased steeply with increasing η_0 up to a value of 25 mPa s and remained constant for higher values. Present theoretical models are not in keeping with the measured data. Modifications of basic model assumptions are suggested.

Key words: biological fluid dynamics, capsule/cell dynamics

1. Introduction

There are multiple reasons to study red blood cells. First, it is of clinical interest because red cells have to traverse the narrow capillaries in the microcirculation, a process which is impaired in certain diseases. Second, it is of biochemical interest because the simple structure of red cells – a single membrane encloses a liquid cytoplasm – simplifies the interpretation of experiments and the study of the relation between structure and function. Third, since computers are becoming more and more powerful, it is a challenge for theorists to model the flow behaviour of red cells in great detail. While the mechanical red cell properties are input parameters of such models, the observed behaviour of the whole red cell serves as a criterion for their verification. Here we present novel data, the results of which could be used to test the physical assumptions underlying those models.

It has long been known that red cells perform two principal motions when their suspension is subjected to shear flow (Goldsmith & Marlow 1972). Below a critical value of the shear rate ($\dot{\gamma}_t$), red cells perform a solid body rotation with little change of their biconcave resting shape. This motion is called tumbling (TB), in accordance with most publications. Above this critical or transition value, the cells become elongated with their long axis including a more or less stationary angle (θ) with the direction

† Email address for correspondence: thmfischer@gmail.com

Name	MW/kD	Company	Lot number	Weight (g)	η_0 (mPa s)
Dextran T 40	41	Pharmacia	2771	1.78	10.7
Dextran FP 60	62	Serva	17 964	1.74	14.6
Dextran 100	100	Serva	B	1.80	23.9
Dextran 500	497	Serva	G9	1.84	55.9
Dextran T 2000	2000	Pharmacia	8122	1.72	104

TABLE 1. Dextrans used in the present study. MW denotes the average molecular weight. Dextran T 2000 was dialysed and freeze-dried before use. Weight is the amount of dextran added to 10 ml of water. Subsequently dextran concentrations were fine-tuned by addition of water. Viscosities were measured at 23 °C.

of the undisturbed flow. In this state, the membrane flows around the oriented red cells, in a motion that has been termed tank-treading (TT) (Schmid-Schönbein & Wells 1969).

In our experiments, the flow of red cell suspensions is observed along the vorticity of a Poiseuille flow through a circular capillary. The cells were suspended in dextran–salt solutions of viscosities (η_0) ranging from 10.7 to 104 mPa s.

2. Materials and methods

2.1. *Preparation of the red cell suspensions*

The sources of dextran are shown in table 1. Dextran solutions were prepared as reported previously (Fischer 2010). In short, dextrans of different molecular weights were dissolved in water. The concentrations (w/v) were the same for all dextrans as controlled by refractometry (Abbe, Zeiss, Oberkochen, Germany). Electrolytes were added as a stock solution of PBS (PBS-Dulbecco 10x, Biochrome, Berlin, Germany). The amount of electrolyte was chosen to preserve the volume the red cells have in blood plasma. To counteract shape changes of red cells, either the echinocytic agent Sulfobetaine SB 12 from Stricker, Tutzing, Germany (concentration 0–10 μM) or the stomatocytic agent human albumin from Sigma-Aldrich, Munich, Germany (concentration 0–4 mg/100 ml) were added to the dextran solutions. The viscosity of the final solutions was measured in a rolling ball viscometer (Anton Paar, Graz, Austria) at 23 °C (table 1).

Blood was obtained on a voluntary basis from regular donors at the local blood bank and aspirated into heparin-containing vacutainers. 1000 μl whole blood were pipetted into an Eppendorf vial, put on ice for 15 min and then centrifuged at 5600 g for 4 min. Supernatant plasma was removed for later addition. Due to the preceding cooling and the rewarming during centrifugation, the buffy coat was rather solid and floated above the red cell column. Therefore it could be aspirated with minimal loss of red cells, thus preserving the characteristic of the population. Finally, plasma was added to obtain a red cell concentration (v/v) of ∼0.5. This suspension was stored on ice. Before an experiment some of it was diluted in three steps 5×10^{-4} times with dextran solution to prepare the final suspension.

2.2. *Experimental protocol*

For details see §§ 1 and 2 of the supplementary material, available at http://dx.doi.org/10.1017/jfm.2013.496. In short, the shape of TT red cells was observed microscopically along the vorticity vector of a Poiseuille flow through a glass capillary

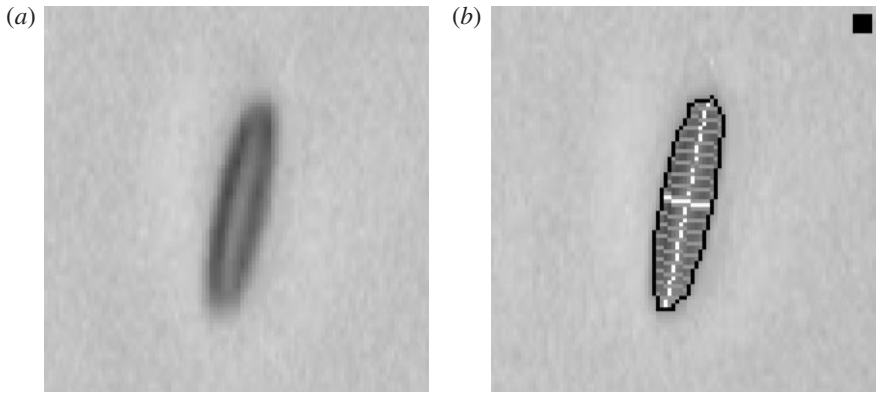

FIGURE 1. (*a*) Microscopic image of a red cell (suspended in a dextran–salt solution of 23.9 mPa s at 23 °C and subjected to a shear flow of 32.4 s^{-1}). (*b*) The same image as (*a*) overlaid first with the principal axes (white), then with the subaxes (grey), and finally with the contour (black). The width of the images corresponds to 23.1 μm. The direction of flow is vertical. The capillary wall is to the left-hand side.

(luminal diameter 975 μm). The flow was driven at constant pressure from a reservoir and varied by more than three orders of magnitude using different resistances at the outflow. The focus of the microscope was set onto the centreline of the capillary. The shape of the red cells was frozen by flash illumination and recorded with an interlaced b/w TV camera. Figure 1(*a*) shows an original image of a TT red cell. A double-flash method with variable distance allowed determination of the velocity of fast as well as slowly flowing objects. The experiments were performed at room temperature (23 °C) and completed within 4 h after blood withdrawal. 44 525 red cells of seven blood samples contributed to this study.

Reports on the mechanical effect of a decrease in red cell adenosine triphosphate (ATP) content are controversial: for recent reports see Tuvia *et al.* (1997), Evans *et al.* (2008), Betz *et al.* (2009), Yoon *et al.* (2009), Park *et al.* (2010) and Boss *et al.* (2012). In our experiments, no measures were taken to change the ATP content. Due to the storage in plasma, the metabolic decrease of ATP is minimized.

The resting shapes of the red cells were assessed subjectively at low flows, both during the experiments and later from the recordings, and categorized according to the scheme of Bessis (1972).

2.3. *Image processing*

The recordings were processed by a custom-made software (see § 3 of the supplementary material for details). In short, a grey-scale threshold converted half-tone images into binary images, i.e. black objects on a white background. The contour of these black objects defined their shape. θ was obtained by determination of the principal axes of all pixels inside and including the contour. The length of the whole cell along the major axis is called L, the thickness along the minor axis is called D. Figure 1(*b*) shows the same image as in figure 1(*a*) but overlaid with the principal axes (white), the subaxes (grey) and the contour (black). From the lengths of the subaxes, measures of the deviation from the symmetry of the objects were calculated and used to exclude malformed cells from the evaluation.

The *apparent* radial position of flowing objects was calculated from their position within the image and the position of the capillary relative to the optical axis of the microscope. The *actual* radial position was derived from the apparent position based on a geometric optics calculation, which accounted for the refraction of light at the curved surfaces between glass and dextran solution. Cells closer to the wall than 50 μm were excluded from the evaluation so that essentially their behaviour in an unbounded shear flow was observed. The shear rate ($\dot{\gamma}$) to which a flowing particle was subjected was determined from its actual radial position (r), its velocity (v) and the luminal radius of the capillary (R). A precondition for this approach is the absence of slip of TT red cells with respect to the undisturbed flow. This absence was demonstrated in extra experiments (see § 7 of the supplementary material).

3. Data processing

The data of each donor were evaluated separately. First, the values of v, collected at a particular outflow resistance, were plotted versus r and fitted parabolically, resulting in a value of $v_{centreline}$. The radial range covered by the microscopic image was subdivided into equal sized bins (r-bins) of width ≈ 2.1 μm. This width is sufficiently small to account for the variation of v due to the parabolic profile. For the centre of each r-bin the respective values for v and $\dot{\gamma}$ were calculated using $v_{centreline}$. Sorting the red cells into the r-bins resulted in their number per bin.

The binned data of all outflow resistances of a certain η_0 were sorted into logarithmically spaced $\dot{\gamma}$-bins. The frequency p_j of red cells observed within a $\dot{\gamma}$-bin with index j was calculated as:

$$p_j = \frac{1}{n_j} \sum_{i=1}^{n_j} \frac{c_i N_i}{f}, \tag{3.1}$$

where n_j is the number of r-bins contributing to the respective $\dot{\gamma}$-bin, N_i is the number of red cells per r-bin, f is the number of film frames of the contributing outflow resistance, and c_i is one of two correction factors. Typically $n_j \approx 60$ for six $\dot{\gamma}$-bins per decade.

The first correction accounts for red cells with low v. In this case the same cell appears in several consecutive frames of the film scene. Therefore, f is reduced to secure statistical independence by

$$c_i = \frac{a}{40\, v}, \tag{3.2}$$

where a is the distance in flow direction covered by the microscopic image but reduced by the average red cell length observed with the respective outflow resistance, and 40 ms is the inverse frame rate of the camera. The correction is applied for

$$v \leqslant \frac{a}{40 + b}, \tag{3.3}$$

where b is the distance between the two flashes. In general, b depends on outflow resistance.

The second correction applies for all other values of v. It accounts for the fact that v can only be evaluated if the cell in question appears on both half-frames of a full frame. This condition reduces the probability of detection. To compensate,

$$c_i = \frac{a}{a - bv}. \tag{3.4}$$

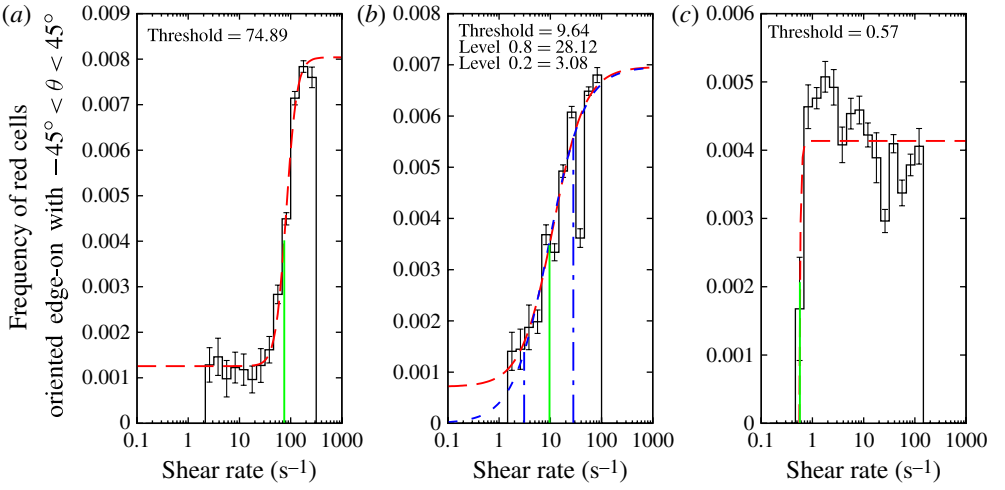

FIGURE 2. (Colour online) Histograms of p_j (equation (3.1)) versus $\dot{\gamma}$ for (*a*) Dx40, (*b*) Dx100 and (*c*) Dx2000. Long-dashed (red) sigmoid in (*a–c*), fit to the experimental histogram (equation (3.5)); short-dashed (blue) sigmoid in (*b*), auxiliary sigmoid for determining Z_t (equation (3.7)); continuous (green) line in (*a–c*), value of $\dot{\gamma}_t$; dash-dotted (blue) lines in (*b*), values of $\hat{\dot{\gamma}}_u$ and $\hat{\dot{\gamma}}_d$. See text for details.

In the experiments, b was chosen small enough to detect a reasonable number of red cells.

Figure 2 shows three examples of histograms of p_j versus $\log(\dot{\gamma})$. In figure 2(*a*) p_j rises from a lower plateau value to a higher one with increasing $\dot{\gamma}$. This step-like behaviour is explained as follows. TT red cells are always oriented edge-on. In this orientation, they present a strong contrast in bright field illumination due to the absorption of haemoglobin. TB red cells, on the other hand, assume all orientations as observed subjectively. Figure 4 in the supplementary material shows a frame with two TB red cells, one oriented edge-on and the other oriented face-on. In addition, TB red cells are known to drift into an orientation in which their axis of symmetry is parallel to the undisturbed vorticity of the flow (Bitbol 1986). This drift would increase the proportion of cells seen face-on. The image processing, in particular the filter for the quality of focus (see § 3, item 7, in the supplementary material), is tuned to detect only cells oriented edge-on. Unless TB red cells happen to have this orientation, they present too little contrast to pass the filter and consequently escape detection. Therefore, the lower plateau is attributed to TB and the higher one to TT.

To obtain a measure for the threshold value $\dot{\gamma}_t$ for the transition from TB to TT, the following sigmoid (long-dashed red in figure 2) was fitted through the histograms:

$$p(\dot{\gamma}) = (p_h - p_\ell)\frac{\left(\dfrac{\dot{\gamma}}{\dot{\gamma}_0}\right)^s}{\left(\dfrac{\dot{\gamma}}{\dot{\gamma}_0}\right)^s + 1} + p_\ell, \tag{3.5}$$

where p_h and p_ℓ are the values of p for the higher and lower plateau value, $\dot{\gamma}_0$ is the value of $\dot{\gamma}$ at the inflection point of the sigmoid, and the exponent s is a measure of the slope at the inflection point. For the purpose of fitting, the weight $\sqrt{\sum_{i=1}^{n_j} N_i}$

was attributed to each column of the histogram. Multiplied by 0.002, these weights are shown as error bars in figure 2. Here $\dot{\gamma}_t$ was obtained via the condition

$$p_t = 0.5 p_h. \tag{3.6}$$

Its value is shown in figure 2 by a continuous (green) line.

The histograms for the high values of η_0, e.g. figure 2(*c*), do not show a clear lower plateau because recordings at outflow resistances with no TT red cells were terminated prematurely in order to save experimental time at extremely low flow rates. The lack of a lower plateau resulted in $p_\ell < 0$ for nine histograms. In these cases, $p_\ell = 0$ was set.

In order to quantify the width of the transition zone (Z_t), an auxiliary sigmoid (short-dashed blue in figure 2*b*) was generated in cases where $p_\ell > 0$. The parameters of this second sigmoid are distinguished by a hat. Three parameters were set: $\hat{p}_\ell = 0$; $\hat{p}_h = p_h$; and $\hat{s}$ was chosen such that the slope at the inflection point remained basically unchanged. $\hat{\dot{\gamma}}_0$ was the only parameter to be fitted. By definition,

$$Z_t = \hat{\dot{\gamma}}_u / \hat{\dot{\gamma}}_d, \tag{3.7}$$

where $\hat{\dot{\gamma}}_u$ and $\hat{\dot{\gamma}}_d$ refer to the values of $\dot{\gamma}$ at the 80 and 20 % level of the auxiliary sigmoid. Their values are shown in figure 2(*b*) by dash-dotted (blue) lines. For clarity, the auxiliary sigmoid and the dash-dotted lines are only shown in figure 2(*b*).

4. Results

In the experiments, it was not possible to tune the red cell shape exclusively to discocyte for several reasons. First, there was always a distribution of different shapes. Second, the donors reacted in different degrees to the same addition of a shape-changing agent. Third, the red cell shape turned out to be very sensitive to small additions of shape-changing agents. Fourth, even the direction of the shape change upon addition of an agent was not always predictable.

The data of all seven blood samples is shown in figure 3 in a double logarithmic plot of the threshold shear stress $\tau_t = \eta_0 \dot{\gamma}_t$ versus η_0. The symbols indicate the average or predominant resting shape of the red cells. Echinocytes, stomatocytes, and discocytes are indicated by stars, lightly filled rings, and full circles, respectively. Stars and filled rings come in three levels of grey-scale value indicating the grade of deviation from the discocyte. The darker the symbol, the smaller the deviation. To give an example, echinocyte I is still biconcave but the rim shows small deviations from circularity whereas echinocyte III is a sphere carrying thick spicules (Bessis 1972).

For two blood samples and two dextran solutions (Dx100 and Dx500), two tests were performed. This was possible because sufficient red cell suspension was left after completion of the standard protocol. In these cases, a minute amount of a shape-changing agent was added to the red cell suspension in the inflow reservoir and the recordings at the first five or six outflow resistances were repeated. The remainder of the recordings were safely above the threshold and were common to both tests. In two of these four cases, the resting shape was changed towards the discocyte. In one case, the change was in the opposite direction. No change occurred in another case. This inconsistent reaction illustrates the difficulty in adjusting the cell shape. The arrows in figure 3 indicate the change in τ_t due to the shape change.

Figure 4 shows Z_t versus η_0. The symbols and arrows have the same meaning as in figure 3. Values of $Z_t > 3.5$ are shown in figure 3 as ranges. The histogram with the widest transition zone is shown in figure 2(*b*). Despite the considerable dispersion of

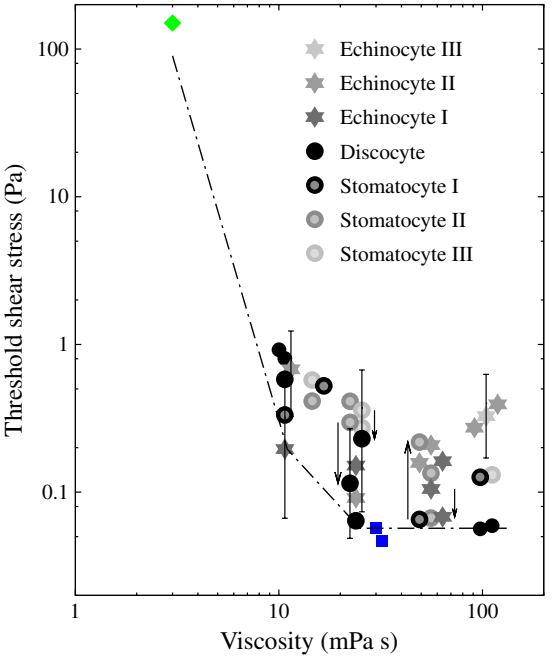

FIGURE 3. (Colour online) Log–log plot of the threshold shear stress $\tau_t = \eta_0 \dot{\gamma}_t$ for the transition from TB to TT of red cells subjected to shear flow versus the viscosity of the suspending phase. Stars, lightly filled rings, and full circles show experimental results of the present work. To distinguish symbols in case of overlap, some of them were shifted slightly parallel to the abscissa. Error bars: width of the zone Z_t (see figure 4). Arrows, change of the threshold shear stress upon changing the resting shape; dash-dotted line, envisaged transition threshold for discocytes; (green) diamond, data of Morris & Williams (1979); (blue) squares, data of Abkarian, Faivre & Viallat (2007). See text for details.

the data, there is a trend to narrower transition zones with increasing values of η_0. The squares in figures 3 and 4 are referred to in §§ 5.1 and 5.2.

5. Discussion

5.1. *Present data*

The experimental data in figure 3 (stars, filled rings and circles) are rather dispersed. Three contributions are suggested. The first is the deviation of the shapes from the discocyte. This is supported by the observed decrease in τ_t (two arrows in figure 3 located at $\eta_0 = 20$ and 30 mPa s) when the shape was changed towards the biconcave disc. The second is an inter-individual variation of red cell properties indicated by the vertical order of the symbols in figure 3 not being exactly in accordance with their degree of deviation from the biconcave shape. The third is statistical variation observable in some histograms, e.g. in figure 2(*b*).

The data in figure 4 are dispersed as well. The width of the transition zone reflects the width of the shape distribution of the red cells. In addition, inter-individual and statistical variations may also contribute.

Despite the scatter in the threshold shear stresses in figure 3, we consider τ_t of a distribution of cell shapes with mainly discocytes to be represented by the lower border of the cloud of experimental points in figure 3. The dash-dotted line in figure 3

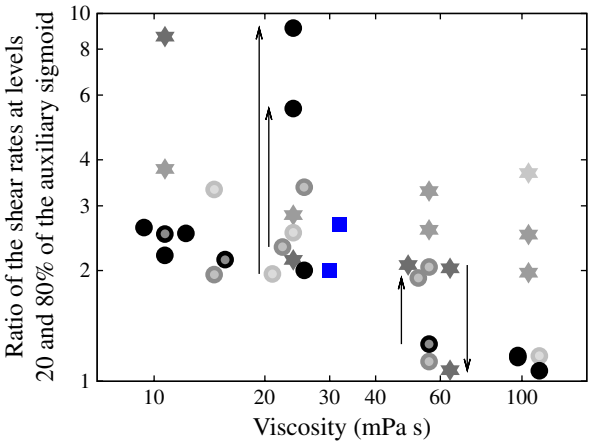

FIGURE 4. (Colour online) Log–log plot of the width of the zone Z_t (equation (3.7)) for the transition from TB to TT of red cells subjected to shear flow versus the viscosity of the suspending phase. Stars, lightly filled rings, and full circles, results of the present work; arrows, change of Z_t upon change in the resting shape; (blue) squares, data of Abkarian *et al.* (2007). See text for details.

approximates our suggestion of the location of this border. In the following, this line is referred to as the transition line. It could be argued that large values of Z_t increase the value of τ_t obtained by fitting. However, figures 3 and 4 show that the transition line is defined by distributions that (i) centre on discocytes and (ii) have minimal values of Z_t.

For $\eta_0 > 25$ mPa s, τ_t is independent of η_0. With decreasing values of η_0, the transition line becomes increasingly steeper. To support this trend, we include data of TT red cells at low elongations (Morris & Williams 1979). These data are shown with a (green) square in figure 3 ($\eta_0 = 3$ mPa s and $L'/W = 1.26$, where L' and W are mean values of red cell length and width, respectively, as observed along the gradient of the undisturbed shear flow).

5.2. *Previous data*

Abkarian *et al.* (2007) observed the transition from TB to TT as well as from TT to TB under three values of η_0 (22, 31 and 47 mPa s). Their data are shown in figures 3 and 4 at $\eta_0 = 30$ mPa s for the transition from TB to TT and at $\eta_0 = 32$ mPa s for the transition from TT to TB. Both the mean values in figure 3 and the width of their distributions in figure 4 are in keeping with our data.

Basu *et al.* (2011) observed $\tau_t = 1.4$ mPa at $\eta_0 = 0.92$ mPa s. They held the red cells stationary within a Poiseuille profile by an optical trap. The following differences to the usual situation of freely floating red cells may explain their extremely low value. First, the red cells are folded due to trapping. Second, in the reference frame of the red cell, the flow above and below the red cell is in the same direction. Third, the forces exerted by the trap itself may foster TT.

5.3. *Factors determining* τ_t

The mechanical behaviour of red cells is determined by intrinsic and extrinsic parameters. In our experiments, neither extrinsic parameters, such as surface area or volume, nor intrinsic parameters, i.e. elastic and viscous constants, were modified. The blood samples were from healthy blood donors. Theoretical modelling, however,

is often a trade-off between computer time and completeness. As a consequence, mechanical properties of red cells known to date may not be accounted for. In addition, not all mechanical properties may be known. Therefore, we discuss the relative importance of the main determinants for τ_t.

In a seminal paper, Keller & Skalak (1982) published a red cell model (KS-model) that described the transition from TB to TT and vice versa upon crossing a threshold in the ratio of the cytoplasmic viscosity (η_{cyt}) and η_0. Instead of accounting for the elastic properties of the red cell membrane, fixed shapes were assumed. The elastic properties, however, endow the membrane with a memory of its shape; for example, parts forming the rim of the discocyte return to the rim after a disturbance of the shape (Fischer 2004). The variations in elastic energy driving this return to a static equilibrium present a barrier to TT, which in turn is responsible for the existence of $\dot{\gamma}_t$.

The red cell membrane hosts two elastic contributions, (i) in bending, and (ii) in two-dimensional shear deformation. The bending stiffness is conferred by the lipid bilayer. Since the lipids are laterally mobile, the reference state in bending has spherical symmetry, i.e. the spontaneous curvature is the same everywhere on the membrane. Therefore, the energy in bending is not responsible for the shape memory. However, the bending stiffness plays an important role in preserving a smooth surface during red cell deformations.

The shear stiffness is conferred by the membrane skeleton, a network of elastic proteins underlying the lipid bilayer. The energy stored in shear depends on the manner in which the proteins of this network are connected. In contrast to the situation in bending, the reference state in shear does not have to have spherical symmetry. Therefore, the shape memory is ascribed to an increase in shear energy upon a deformation and $\dot{\gamma}_t$ is expected to be strongly dependent on the amplitude (E_0) of the variations in shear energy during TT.

In some models, the external space is confined by a fluid box. A decrease of its size in the direction of the undisturbed gradient has been shown theoretically to favour TT over TB (Kaoui, Kruger & Harting 2012). This effect has also been observed experimentally in a cone-plate chamber (unpublished observations).

There is no simple way to predict the influence of cellular viscosities on the transition from TB to TT. Fischer & Korzeniewski (2011) studied the elongation of TT red cells varying $\dot{\gamma}$ and η_0. They found a threshold in η_0 above which the elongation was independent of cellular viscosities. Below the threshold, the influence of energy dissipation within the red cell increased with decreasing η_0. A similar influence is expected in the transition from TB to TT.

5.4. *Fixed-shape models*

Skotheim & Secomb (2007) added an oscillating energy term to the KS model to account for the elasticity of the membrane. An oblate spheroid with a principal axis ratio of four was taken as a model for a biconcave red cell. The amplitude E_0 of the oscillating energy term was evaluated as 10^{-17} J based on experiments of Fischer (2004). The viscosity of the membrane (η_{mem}) was indirectly accounted for by increasing η_{cyt} by a factor of four.

Between TB and TT an intermediate region was found (see the range in figure 5) in which TB and TT took turns. Although it has been shown that this behaviour is due to the assumption of a fixed shape (Vlahovska *et al.* 2011), the intermediate region nevertheless indicates the location of the transition region.

Noguchi (2009), using essentially the same model but covering a range of external viscosities, found an intermediate region characterized by synchronized motions of TB

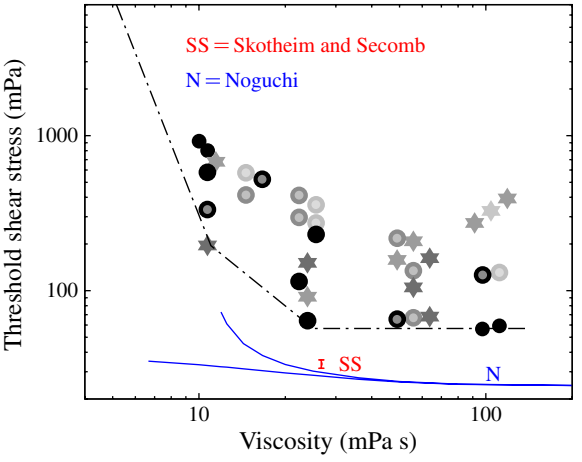

FIGURE 5. (Colour online) Log–log plot of the threshold shear stress $\tau_t = \eta_0 \dot{\gamma}_t$ for the transition from TB to TT of red cells subjected to shear flow versus the viscosity of the suspending phase. Symbols, experimental results of the present work; dash-dotted line, envisaged transition threshold for discocytes; continuous (blue) lines and (red) range, theoretical results from fixed-shape models. See § 5.4 for details.

and TT. The two borders lining this region are shown in figure 5. They coalesce for $\eta_0 > 40$ mPa s. E_0 was obtained by comparison to a static tweezer experiment, and a value slightly lower than that of Skotheim & Secomb (2007) was found. Accordingly, Noguchi's values of the intermediate region are somewhat lower than those of Skotheim and Secomb (figure 5).

The fixed shape in both models, although not biconcave, is concordant with the observation that the red cell shape is preserved during the transition from TB to TT (Dupire, Socol & Viallat 2012). Noguchi's model captures the increase of τ_t with decreasing values of η_0. Both models could be reconciled with the experiments by choosing a higher value of E_0.

Abkarian *et al.* (2007) also used the KS model. To fit their own experimental data, they used a Kelvin–Voigt model to account for the shear elasticity and viscosity of the membrane. The result of their fit was a shear modulus ranging from 0.007 to 0.1 μN m^{-1}, two to three orders of magnitude below the accepted value. The cause of this discrepancy may lie in the use of the membrane flow as given by the KS model. Its streamlines lie in planes normal to the undisturbed vorticity. Real streamlines are curved, as observed experimentally (unpublished observations) as well as demonstrated theoretically (Secomb & Skalak 1982). While the flow field of the KS model may lead to reasonable estimates for the cytoplasmic dissipation, it produces large membrane deformations in those regions where the intermediate principal axis of the ellipsoid meets the membrane. Since the actual fitted quantity is E_0, an increase in local shear deformation is expected to be compensated by a decrease in the shear modulus.

5.5. *Discrete models*

Discrete models subdivide the membrane into small triangles. In this way, almost any shape can be modelled depending on the number of vertices at the corners of the triangles.

Models with membranes without bending stiffness show intensely folded surfaces during TT (Le & Tan 2010; Huang, Chang & Sung 2012). Such models are not

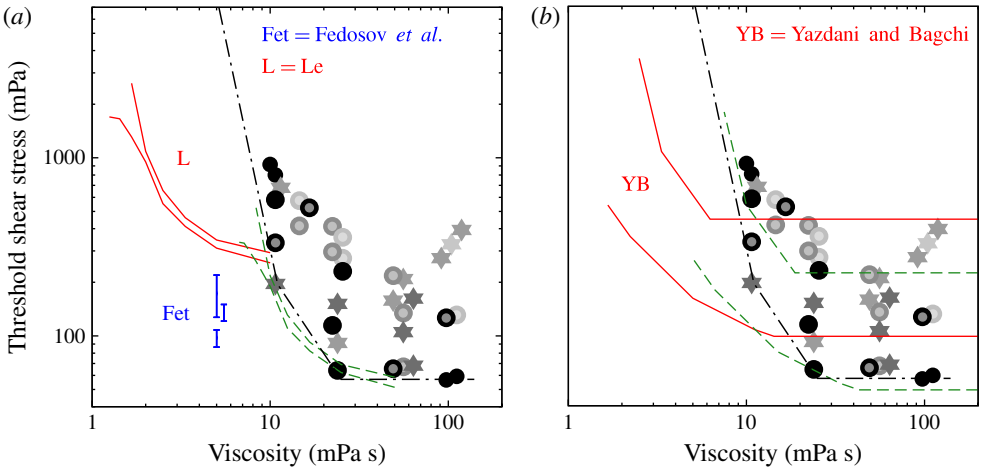

FIGURE 6. (Colour online) Log–log plot of the threshold shear stress $\tau_t = \eta_0 \dot{\gamma}_t$ for the transition from TB to TT of red cells subjected to shear flow versus the viscosity of the suspending phase. Symbols, experimental results of the present work; dash-dotted line, envisaged transition threshold for discocytes; continuous (red) lines and (blue) ranges, theoretical results from discrete models; dashed (green) lines, theoretical results after a suggested modification. See § 5.5 for details.

considered here for two reasons. First, the normal red cell membrane does not buckle, either upon swelling or during TT (Fischer *et al.* 1981). Second, a buckling membrane avoids storage of elastic shear energy at the expense of the bending energy. Thus, buckling observed in a theoretical model is expected to decrease τ_t.

The models of Le (2010) and Yazdani & Bagchi (2011) are similar. The number of vertices is $\approx 10^4$, i.e. fine graining. For the membrane shear elasticity, they use the constitutive equation of Skalak *et al.* (1973). The reference shape is the discocyte published by Evans & Fung (1972). The membrane is provided with bending stiffness but is without viscosity. Differences concern the size of the fluid box and the reference shape for the bending elasticity.

The results of both models are given in dimensionless form as functions of $\lambda = \eta_{cyt}/\eta_0$, $C_n = \dot{\gamma}\eta_0 a_0/E_s$, and $K_b = \kappa_b/a_0^2 E_s$, where $a_0 = (3V/4\pi)^{1/3}$, V is the red cell volume, κ_b is the bending stiffness, and E_s is the membrane shear modulus. Note that $E_s = 2G_s$, where G_s is the shear modulus as defined by Dimitrakopoulos (2012). With $V = 94\ \mu\text{m}^3$, η_{cyt}, and G_s, we calculated the values of η_0, $\dot{\gamma}$ and κ_b.

First, we used $\eta_{cyt} = 10\,\text{mPa s}$, the value at room temperature, and $G_s = 2.5\ \mu\text{N m}^{-1}$, the best choice when the constitutive equation of Skalak *et al.* (1973) is used (Dimitrakopoulos 2012). Among the values for K_b used by both authors, we selected the one resulting in $\kappa_b = 4 \times 10^{-19}$ J. Both models give a transition region located between pure TB and pure TT. The borders lining these regions are shown in figure 6(*a,b*) as continuous (red) lines. The region of D.-V. Le (personal communication) is much narrower than that of Yazdani & Bagchi (2011). A cause of this difference might be the reference shapes for bending. Yazdani and Bagchi use a uniform, negative spontaneous curvature whereas Le uses the discocyte as the reference shape.

The shapes in the transition region shown by Yazdani & Bagchi (2011) may be summarized from the perspective of TT without loss of the dimples. The dimples

References	η^m_{cyt} mPas	D^m_{mem}/D^m_{cyt}	G^m_s μN m^{-1}	$E^\star_0$	d_w μm	κ^m_b 10^{-19} J
Yazdani & Bagchi (2011)	30	2	1.25	2	18	2
Le (2010, personal communication)	50	4	0.5	5	28	0.8

TABLE 2. η^m_{cyt} and G^m_s are the values chosen to accomplish a match of two theoretical models with the present experimental results. D^m_{mem} and D^m_{cyt} denote the rate of energy dissipation in the membrane and cytoplasm of a TT red cell, respectively. $E^\star_0 = 2.5\ \mu\text{N m}^{-1}/G^m_s$ is a relative measure for the value of E_0 before the match was performed. d_w is the size of the fluid box in the direction of the undisturbed gradient. κ^m_b is the value after the match.

are not stationary as described by Dupire *et al.* (2012) but rather travel with the TT membrane and become periodically quite deep. This situation resembles the behaviour of a curved column under compression in that under increasing loads the column increases its native curvature.

Increasing κ_b by a factor of five, the transition region in figure 6(*b*) collapses to a single line close to the lower border (Yazdani & Bagchi 2011). This confirms that the bending stiffness suppresses strong curvatures but does not influence τ_t. From the collapse one might conclude that $\kappa_b = 4 \times 10^{-19}$ J was chosen too low. Most recent experimental determinations of κ_b, however, range from 2.7×10^{-19} J to 3.3×10^{-19} J (Betz *et al.* 2009; Yoon *et al.* 2009; Boss *et al.* 2012) with a single one at 8.1×10^{-19} J (Evans *et al.* 2008). One way to keep the value of κ_b without the occurrence of travelling dimples is discussed in § 5.7.

In the next step we follow the strategy of Skotheim & Secomb (2007) and increase η_{cyt} to account for the viscosity of the membrane. This leads to a pure right-shift of the transition regions. To bring the theories into agreement with the experiments requires an additional down-shift. Generally speaking, this is achieved by decreasing E_0. Within the framework of the two models it can only be accomplished by decreasing G_s. The final positions of the transition regions are shown by the dashed (green) lines in figure 6(*a*,*b*). Because of the absence of an influence of the bending stiffness on τ_t we chose the lower border of the transition region to coincide with the experimental transition line in figure 6(*b*).

Table 2 shows the values after the shift. They are distinguished by an upper index '*m*'. The ratios of the rates of energy dissipation (D^m) in the membrane and cytoplasm are in keeping with the range of values in the literature (Fischer 1980; Secomb & Skalak 1982; Tran-Son-Tay, Sutera & Rao 1984). The values of G^m_s, on the other hand, are appreciably lower than the well-established experimental value (see references in Dimitrakopoulos 2012). Another way to decrease E_0 while keeping the accepted value of $G_s = 2.5\ \mu\text{N m}^{-1}$ is discussed in § 5.7.

The lower G^m_s, the higher is E_0 in the respective model. For the sake of comparison we calculate $E^\star_0 = 2.5\ \mu\text{N m}^{-1}/G^m_s$ as a relative measure for E_0 (table 2). The values of $E^\star_0$ for the two models are quite different (table 2). To some extent this can be explained by the size of the respective fluid boxes. The stronger the confinement, i.e. the smaller the fluid box, the smaller should be E_0, in keeping with the numbers of $E^\star_0$ in table 2.

Fedosov, Caswell & Karniadakis (2010*b*) used 500 vertices, i.e. a coarse-grained model. It is a so-called multiscale model which starts from the viscoelastic properties of the springs connecting the vertices. The choice of its intrinsic parameters resulted

in a shear modulus of 6.3 μN m^{-1}, a bending stiffness of 2.4×10^{-19} J, and a three-dimensional membrane viscosity of 22 mPa s; η_0 and η_{cyt} were both set to 5 mPa s.

The authors did not find intermittency but a region of indeterminacy in which the model showed neither pure TB nor pure TT (D. A. Fedosov, personal communication). The widths of these regions are shown in figure 6(*a*) as (blue) ranges. The largest range is obtained by accounting for both sources of viscosity. The one displaced horizontally accounts only for the cytoplasmic viscosity. The lowest range is without any viscosity. $E_0 = 3$–3.5×10^{-17} J (Fedosov, Caswell & Karniadakis 2010*a*) is in keeping with the much higher value of these authors for τ_t compared to the results of Skotheim & Secomb (2007) and Noguchi (2009).

It is difficult to pinpoint the cause of the discrepancy with the experiments since the effective constitutive equation is not known. Further, although buckling was observed in the region of indeterminacy as well as in its neighbourhood, its influence on τ_t is not evident due to coarse-graining. The gap between the walls generating the shear flow was 20 μm (Fedosov, personal communication). Confinement could therefore account for some of the discrepancy. The main cause is probably the mismatch between η_{cyt} and the intrinsic parameters of the membrane. These parameters have values appropriate for room temperature whereas $\eta_{cyt} = 5$ mPa s is less than the value at 37 °C. Increasing η_{cyt} might increase η_0 concurrently and in this way move the ranges closer to the transition line.

5.6. *Membrane viscosity*

Accounting for η_{mem} indirectly by increasing η_{cyt} is successful, but fitting models which explicitly account for η_{mem} would allow us to determine its value. The part of the transition line where it shows a steep slope depends on the cellular viscosities, in contrast to the part where it is horizontal. Including η_{mem} in continuum models might also resolve the contradiction between the result of Fedosov *et al.* (2010*b*), who found a weak dependence on cellular viscosities and the strong influence suggested by fitting two other models to the experiments (see figure 6*a,b*). It may further decide between the conflicting values of η_{mem} found with pipette methods (Hochmuth, Worthy & Evans 1979; Linderkamp & Meiselman 1982), on one hand, and the fit to the KS model (Tran-Son-Tay *et al.* 1984), on the other hand. It is mentioned here that the determination of η_{mem} performed by Tran-Son-Tay *et al.* (1984) suffers from the same artifact of straight streamlines mentioned in § 5.4.

5.7. *Stress-free shape*

There are two extreme cases for a stress-free or reference shape for the shear elasticity: (i) the sphere and (ii) the biconcave resting shape. In case (i), $E_0 = 0$. For intermediate shapes between the discocyte and the sphere, $E_0 > 0$ but smaller than in case (ii). Therefore, instead of decreasing G_s and κ_b, the choice of an intermediate reference shape is an alternative way to reduce E_0. In contrast to the situation for η_{mem}, it is the horizontal part of the transition line which is best suited for a fit of the reference shape to the experiments.

Besides shifting the transition regions downwards, an intermediate stress-free shape without dimples is expected to have the additional benefit of abolishing travelling dimples. Thus it will shrink or even remove the transition region between TB and TT with κ_b closer to experimental values. Further, it should be interesting to see whether the reference shape resulting from such a fit is similar to the reference shape used by Lim, Wortis & Mukhopadhyay (2002) in their static model. The ultimate check concerns the resting shape: it should be close to that of red cells in blood plasma.

Besides the search for an intermediate stress-free shape, the more general concept of a deformation state (Fischer 2004) that accounts for the shear history of red cells in the circulation might be considered.

Acknowledgements

The authors thank the staff of the blood bank, Universitätsklinikum Aachen, for their cooperation in placing the blood samples at our disposal, the staff of the mechanical workshop, Universitätsklinikum Aachen, for helping along the way, Dipl. Ing. M. Laumen, RWTH-Aachen, for the opportunity to perform the viscometric measurements in his laboratory, Drs D. Abreu and U. Seifert, University of Stuttgart, Germany, for enlightening discussions, Dr D. V. Le for communicating unpublished results, Drs A. Yazdani and P. Bagchi for communicating numerical results and for pointing out that different definitions of the shear modulus are in use, and finally the referees, whose comments helped to improve the manuscript considerably. The capillaries were a gracious sample delivery from Hilgenberg GmbH, Malsfeld, Germany.

Supplementary material

Supplementary material are available at http://dx.doi.org/10.1017/jfm.2013.496.

REFERENCES

ABKARIAN, M., FAIVRE, M. & VIALLAT, A. 2007 Swinging of red blood cells under shear flow. *Phys. Rev. Lett.* **98**, 188302.

BASU, H, DHARMADHIKARI, A. K., DHARMADHIKARI, J. A., SHARMA, S. & MATHUR, D. 2011 Tank treading of optically trapped red blood cells in shear flow. *Biophys. J.* **101**, 1604–1612.

BESSIS, M. 1972 Red cell shapes: an illustrated classification and its rationale. *Nouvelle Revue Française d'Hématologie* **12**, 721–746.

BETZ, T., LENZ, M., JOANNY, J.-F. & SYKES, C. 2009 ATP-dependent mechanics of red blood cells. *Proc. Natl Acad. Sci.* **106**, 15320–15325.

BITBOL, M. 1986 Red blood cell orientation in orbit $C = 0$. *Biophys. J.* **49**, 1055–1068.

BOSS, D., HOFFMANN, A., RAPPAZ, B., DEPEURSINGE, C. & MAGISTRETTI, P. J. 2012 Spatially-resolved eigenmode decomposition of red blood cells membrane fluctuations questions the role of ATP in flickering. *PLoS ONE* **7**, e40667.

DIMITRAKOPOULOS, P. 2012 Analysis of the variation in the determination of the shear modulus of the erythrocyte membrane: effects of the constitutive law and membrane modelling. *Phys. Rev.* E **85**, 041917.

DUPIRE, J., SOCOL, M. & VIALLAT, A. 2012 Full dynamics of a red blood cell in shear flow. *Proc. Natl Acad. Sci. USA* **109**, 20808–20813.

EVANS, E. & FUNG, Y.-C. 1972 Improved measurements of the erythrocyte geometry. *Microvasc. Res.* **4**, 335–347.

EVANS, J., GRATZER, W., MOHANDAS, N., PARKER, K. & SLEEP, J. 2008 Fluctuations of the red blood cell membrane: relation to mechanical properties and lack of ATP dependence. *Biophys. J.* **94**, 4134–4144.

FEDOSOV, D. A., CASWELL, B. & KARNIADAKIS, G. E 2010*a* Dissipative particle dynamics modelling of red blood cells. In *Red Cell Membrane Transport in Health and Disease* (ed. C. Pozrikidis), pp. 182–218. CRC Press.

FEDOSOV, D. A., CASWELL, B. & KARNIADAKIS, G. E. 2010*b* A multiscale red blood cell model with accurate mechanics, rheology, and dynamics. *Biophys. J.* **98**, 2215–2225.

FISCHER, T. M. 1980 On the energy dissipation in a tank-treading human red blood cell. *Biophys. J.* **61**, 863–868.

FISCHER, T. M. 2004 Shape memory of human red blood cells. *Biophys. J.* **86**, 3304–3313.

FISCHER, T. M. 2010 A method to prepare isotonic dextran–salt solutions. *Cytometry* A **77**, 805–810.

FISCHER, T. M., HAEST, C. W. M., STÖHR-LIESEN, M., SCHMID-SCHÖNBEIN, H. & SKALAK, R. 1981 The stress-free shape of the red blood cell membrane. *Biophys. J.* **34**, 409–422.

FISCHER, T. M. & KORZENIEWSKI, R. 2011 Effects of shear rate and suspending medium viscosity on elongation of red cells tank-treading in shear flow. *Cytometry* A **79**, 946–951.

GOLDSMITH, H. L. & MARLOW, J. 1972 Flow behaviour of erythrocytes. Part 1. Rotation and deformation in dilute suspensions. *Proc. R. Soc. Lond.* B **182**, 351–384.

HOCHMUTH, R. M., WORTHY, P. R. & EVANS, E. A. 1979 Red cell extensional recovery and the determination of membrane viscosity. *Biophys. J.* **26**, 101–114.

HUANG, W.-X., CHANG, C. B. & SUNG, H. J. 2012 Three-dimensional simulation of elastic capsules in shear flow by the penalty immersed boundary method. *J. Comput. Phys.* **231**, 3340–3364.

KAOUI, B., KRUGER, T. & HARTING, J. 2012 How does confinement affect the dynamics of viscous vesicles and red blood cells?. *Soft Matt.* **8**, 9246–9252.

KELLER, S. R. & SKALAK, R. 1982 Motion of a tank-treading ellipsoidal particle in a shear flow. *J. Fluid Mech.* **120**, 27–47.

LE, D. V. 2010 Effect of bending stiffness on the deformation of liquid capsules enclosed by thin shells in shear flow. *Phys. Rev.* E **82**, 016318.

LE, D.-V. & TAN, Z. 2010 Large deformation of liquid capsules enclosed by thin shells immersed in the fluid. *J. Comput. Phys.* **229**, 4097–4116.

LIM, G. H. W., WORTIS, M. & MUKHOPADHYAY, R. 2002 Stomatocyte–discocyte–echinocyte sequence of the human red blood cell: evidence for the bilayer-couple hypothesis from membrane mechanics. *Proc. Natl Acad. Sci. USA* **99**, 16766–16769.

LINDERKAMP, O. & MEISELMAN, H. J. 1982 Geometric, osmotic, and membrane mechanical properties of density-separated human red cells. *Blood* **59**, 1121–1127.

MORRIS, D. R. & WILLIAMS, A. R. 1979 The effects of suspending medium viscosity on erythrocyte deformation and haemolysis *in vitro*. *Biochim. Biophys. Acta* **550**, 288–296.

NOGUCHI, H. 2009 Swinging and synchronized rotations of red blood cells in simple shear flow. *Phys. Rev.* E **80**, 021902.

PARK, Y., BEST, C. A., BADIZADEGAN, K., DASARI, R. R., FELD, M. S., KURIABOVA, T., HENLE, M. L., LEVINE, A. J. & POPESCU, G. 2010 Measurement of red blood cell mechanics during morphological changes. *Proc. Natl Acad. Sci.* **107**, 6731–6736.

SCHMID-SCHÖNBEIN, H. & WELLS, R. 1969 Fluid drop-like transition of erythrocytes under shear. *Science* **165**, 288–291.

SECOMB, T. W. & SKALAK, R. 1982 Surface flow of viscoelastic membranes in viscous fluids. *Q. J. Mech. Appl. Maths* **35**, 233–247.

SKALAK, R., TÖZEREN, A., ZARDA, P. & CHIEN, S. 1973 Strain energy function of red blood cell membranes. *Biophys. J.* **13**, 245–264.

SKOTHEIM, J. M. & SECOMB, T. W. 2007 Red blood cells and other nonspherical capsules in shear flow: oscillatory dynamics and the tank-treading-to-tumbling transition. *Phys. Rev. Lett.* **98**, 078301.

TRAN-SON-TAY, R., SUTERA, S. P. & RAO, P. R. 1984 Determination of red blood cell membrane viscosity from rheoscopic observations of tank-treading motion. *Biophys. J.* **46**, 65–72.

TUVIA, S., ALMAGOR, A., BITLER, A., LEVIN, S., KORENSTEIN, R. & YEDGAR, S. 1997 Cell membrane fluctuations are regulated by medium macroviscosity: evidence for a metabolic driving force. *Proc. Natl Acad. Sci. USA* **94**, 5045–5049.

VLAHOVSKA, P. M., YOUNG, Y.-N., DANKER, G. & MISBAH, C. 2011 Dynamics of a non-spherical microcapsule with incompressible interface in shear flow. *J. Fluid Mech.* **678**, 221–247.

YAZDANI, A. Z. K. & BAGCHI, P. 2011 Phase diagram and breathing dynamics of a single red blood cell and a biconcave capsule in dilute shear flow. *Phys. Rev.* E **84**, 026314.

YOON, Y.-Z., HONG, H., BROWN, A., KIM, D. C., KANG, D. J., LEW, V. L. & CICUTA, P. 2009 Flickering analysis of erythrocyte mechanical properties: dependence on oxygenation level, cell shape, and hydration level. *Biophys. J.* **97**, 1606–1615.